

## SCALING LAWS FOR ADVECTION-DOMINATED FLOWS: APPLICATIONS TO LOW-LUMINOSITY GALACTIC NUCLEI

ROHAN MAHADEVAN

Harvard-Smithsonian Center for Astrophysics, 60 Garden Street, Cambridge, MA 02138

Received 1996 April 26; accepted 1996 September 23

### ABSTRACT

We present analytical scaling laws for self-similar advection-dominated flows. The spectra from these systems range from  $10^8$  to  $10^{20}$  Hz and are determined by considering cooling of electrons through synchrotron, bremsstrahlung, and Compton processes. We show that the spectra can be quite accurately reproduced without detailed numerical calculations and that there is a strong testable correlation between the radio and X-ray fluxes from these systems. We describe how different regions of the spectrum scale with the mass of the accreting black hole,  $M$ , the accretion rate of the gas,  $\dot{M}$ , and the equilibrium temperature of the electrons,  $T_e$ . We show that the universal radio spectral index of 1/3 observed in most elliptical galaxies (Slee et al.) is a natural consequence of self-absorbed synchrotron radiation from these flows. We also give expressions for the total luminosity of these flows and the critical accretion rate,  $\dot{M}_{\text{crit}}$ , above which the advection solutions cease to exist. We find that for most cases of interest, the equilibrium electron temperature is fairly insensitive to  $M$ ,  $\dot{M}$ , and parameters in the model. We apply these results to low-luminosity black holes in galactic nuclei. We show that the problem posed by Fabian & Canizares of whether bright elliptical galaxies host dead quasars is resolved, as pointed out recently by Fabian & Rees, by considering advection-dominated flows.

*Subject headings:* accretion, accretion disks — black hole physics — cooling flows — galaxies: elliptical and lenticular, cD — radiation mechanisms: thermal — radio continuum: galaxies — X-rays: galaxies

### 1. INTRODUCTION

The observational proof for the existence of black holes is one of the outstanding problems in astrophysics today. It is generally believed that black holes exist in binary star systems, at the centers of most normal galaxies, and are the central engines that power distant quasars. Attempts to prove the existence of these singularities are confined to inferring their presence by observing how they affect their environment. Measuring the kinematics of stellar systems and gas orbiting near the cores of galaxies (see, e.g., van den Bosch & van der Marel 1995; van der Marel 1995), using time variability arguments of the X-ray fluxes from quasars (e.g., see Wandel & Mushotzky 1986), or measuring the mass function in X-ray binaries (see, e.g., Haswell et al. 1993) are ways of inferring the existence of a massive object (black hole) that is confined to a small volume.

Another way of inferring the presence of a black hole is to consider the emission spectrum produced by an accretion disk as the surrounding gas accretes onto the central object. The standard theory of accretion disks has serious difficulties in explaining the entire spectrum of black hole systems. The primary problem in the standard thin disk models is that the accreting gas is optically thick and radiates locally as a modified blackbody spectrum (see Frank, King, & Raine 1992). This simple spectrum clearly falls short of explaining the entire emission from the radio to hard X-rays of these systems. Models have been proposed that explain the emission spectrum at certain frequencies (see, e.g., Duschl & Lesch 1994), but these fail to explain the emission in other regions of the spectrum.

A possibility of explaining the entire spectrum of these systems has recently emerged with the consideration of advection-dominated accretion (Narayan & Yi 1994, 1995a, 1995b; Abramowicz et al. 1995; Abramowicz et al. 1988; Rees et al. 1982). Unlike standard accretion disk theory, one class of advection-dominated accretion considers accretion flows that are optically thin and have low radiative efficiency. These flows have a two-temperature structure (Shapiro, Lightman, & Eardley 1976) and hence do not require all the viscously dissipated energy to be radiated locally but instead allow a large fraction of the generated energy to be advected inward, with the flow, to be deposited ultimately into the black hole. The total luminosity from these disks is therefore much lower, for a fixed accretion rate, than the luminosity from a thin accretion disk. It is, however, also possible to have a disk structure where there is an outer thin disk, which becomes advection-dominated as the flow approaches the black hole. In this case the outer disk gives the standard modified blackbody spectrum (Frank et al. 1992) that produces standard thin disk luminosities (see, e.g., Narayan 1996; Narayan, McClintock, & Yi 1996a; Lasota et al. 1996). For the present discussion, we neglect the outer disk component since standard thin disks are well understood and we are mainly interested in the advection-dominated flow.

The optically thin accretion flows in advection-dominated systems naturally require electrons in the gas to cool via synchrotron, bremsstrahlung, and inverse Compton processes. These processes are responsible for producing the entire spectrum, in these systems, from the radio to hard X-rays, in a natural way. A unique feature in considering advection flows to describe accreting black hole systems is that they *require* the existence of an event horizon (Narayan, Yi, & Mahadevan 1996b; Narayan et al. 1996a), since a hard surface (e.g., a neutron star) would reradiate all the advected energy, thereby producing an equivalent total luminosity as predicted by a thin accretion disk. Successful application of these models to black hole systems might therefore prove the existence of an event horizon (Narayan, Yi, & Mahadevan 1995; Narayan et al. 1996a).

Detailed numerical calculations that consider the individual cooling and heating processes in the flow have been performed by Narayan & Yi (1995b), and the resulting spectra have been successfully applied to a number of putative black hole systems

(see, e.g., Narayan et al. 1995; Lasota et al. 1996; Narayan et al. 1996a). Narayan & Yi (1995b) have numerically obtained a number of interesting properties of these advection flows. From the detailed calculations, however, it is difficult to deduce how different regions of a spectrum scale as quantities such as the mass of the central object and accretion rate are varied.

The present paper develops analytical expressions to describe the general properties of advection-dominated flows. We deduce scaling laws that give physical insight to the detail processes involved and show how these simple laws give rise to quite an accurate description of these flows. In § 2 we review the self-similar flow equations for advection dominated disks. Section 3 describes the heating and cooling processes, and § 4 shows how the entire spectrum from these systems can be understood by simple scaling laws. Section 5 addresses the general properties of the flow. In § 6 we follow Fabian & Rees (1995) and apply the results to resolve the long-standing problem posed by Fabian & Canizares (1988) of whether elliptical galaxies host dead quasars. Finally, in § 7, we discuss future applications of these models and conclude.

## 2. SELF-SIMILAR FLOW EQUATIONS

In this section we review some of the basic assumptions and equations of the self-similar advection-dominated models developed by Narayan & Yi (1995b). Narayan & Yi (1995b) present self-similar equations that describe local properties of the accreting gas as a function of the mass,  $M$ , the accretion rate,  $\dot{M}$ , the radius,  $R$ , the viscosity parameter,  $\alpha$ , the ratio of gas pressure to total pressure,  $\beta$ , and the fraction of viscously dissipated energy that is advected,  $f$ .

The accreting gas in an advection-dominated flow is a two-temperature optically thin plasma. The ions are at their virial temperature, and the electrons are significantly cooler. The total pressure,  $p$ , in these flows is the sum of gas ( $p_g$ ) and magnetic ( $p_m$ ) pressure. The gas is roughly in equipartition with an isotropically tangled magnetic field,  $B$ , which contributes a factor  $1 - \beta$  to the total pressure,

$$p_m \equiv (1 - \beta)\rho c_s^2 = \frac{B^2}{24\pi}. \quad (1)$$

This equation differs that of from Narayan & Yi (1995b) by a factor of one-third to account for the pressure due to a three-dimensional tangled magnetic field.  $\rho$  and  $c_s$  are the mass density and speed of sound.

The self-similar equations are written in terms of scaled quantities: the mass is scaled in solar mass units

$$M = mM_\odot, \quad (2)$$

the radius in Schwarzschild radii

$$R = rR_{\text{Schw}}, \quad R_{\text{Schw}} = \frac{2GM}{c^2} = 2.95 \times 10^5 m \text{ cm}, \quad (3)$$

and the accretion rate in Eddington units

$$\begin{aligned} \dot{M} &= \dot{m}\dot{M}_{\text{Edd}}, \\ \dot{M}_{\text{Edd}} &= \frac{L_{\text{Edd}}}{\eta_{\text{eff}} c^2} = 1.39 \times 10^{18} m \text{ g s}^{-1}, \end{aligned} \quad (4)$$

where  $\eta_{\text{eff}} = 0.1$  is the standard efficiency in converting matter to energy (Frank et al. 1992).

Since these flows are essentially spherical in geometry (Narayan & Yi 1995b), the vertical scale height of the disk is set equal to the radius in the equations that follow. With this approximation and the scalings above, the self-similar equations for the accretion flow which are relevant for the present discussion are (Narayan & Yi 1995b)

$$\begin{aligned} \rho &= 6.00 \times 10^{-5} \alpha^{-1} c_1^{-1} \dot{m}^{-1} \dot{m} r^{-3/2} \text{ g cm}^{-3}, \\ B &= s_1 \dot{m}^{-1/2} \dot{m}^{1/2} r^{-5/4} \text{ G}, \\ n_e &= b_1 \dot{m}^{-1} \dot{m} r^{-3/2} \text{ cm}^{-3}, \\ s_1 &= 1.42 \times 10^9 \alpha^{-1/2} (1 - \beta)^{1/2} c_1^{-1/2} c_3^{1/2}, \\ b_1 &= 3.16 \times 10^{19} \alpha^{-1} c_1^{-1}. \end{aligned} \quad (5)$$

These are the equations that differ from those of Narayan & Yi (1995b) since we have assumed spherical accretion.  $n_e$  is the number density of electrons, and  $c_1$ ,  $c_3$  are constants as defined in Narayan & Yi (1995b).<sup>1</sup> For all cases of interest,  $c_1 \simeq 0.5$  and  $c_3 \simeq 0.3$ .

## 3. ENERGY BALANCE AND HEATING OF A TWO-TEMPERATURE PLASMA

The accreting gas in the advection flows is heated locally by viscous forces. In the analysis of Narayan & Yi (1995b), the viscously dissipated energy  $q^+$  is mainly transferred to the ions in the gas. A fraction  $f$  of this energy is carried inward by the accreting gas, while the remaining fraction  $1 - f$  is transferred from the ions to the electrons to be radiated via synchrotron, inverse-Compton, and bremsstrahlung emission. There are therefore two energy equations that need to be satisfied. In the

<sup>1</sup> In the definition of  $c_1$ ,  $c_3$  as given in Narayan & Yi (1995b), the ratio of specific heats of the gas is different from the present paper. We use (Esin 1997)  $\gamma = (8 - 3\beta)/(6 - 3\beta)$ .

present analysis, we account for the possibility of viscously heating the electrons by a fraction  $\delta$ . Since the heat generated by the viscous forces is transferred mainly to those particles with more inertial mass, we would expect that the fraction  $\delta$  of viscous energy transferred to the electrons is in the ratio of the electron to ion mass  $\sim m_e/m_i \sim 1/2000$ . The energy balance for the ions therefore satisfies

$$\begin{aligned} q^+ &= f q^+ + q^{ie} + \delta q^+, \\ &\equiv q^{\text{adv}} + q^{e+} \text{ ergs s}^{-1} \text{ cm}^{-3}, \end{aligned} \quad (6)$$

with

$$\begin{aligned} q^{\text{adv}} &\equiv f q^+, \\ q^{e+} &\equiv q^{ie} + \delta q^+. \end{aligned}$$

Here,  $q^+$  and  $q^{ie}$  are the rate of heating per unit volume and rate of transfer of energy from the ions to the electrons per unit volume respectively,  $q^{\text{adv}}$  is the advected energy, and  $q^{e+}$  is total electron heating rate including viscous heating.

The electrons satisfy the energy equation,  $q^{e+} = q^-$ , where  $q^-$  is the sum of all the local cooling processes (synchrotron, bremsstrahlung, and inverse-Compton). Setting  $\delta = 0$  in these equations gives the energy equations of Narayan & Yi (1995b). For a given  $m, \dot{m}, r, \alpha$ , and  $\beta$ , the electron and ion energy equations are solved to determine the electron and ion temperatures of the plasma and to determine the fraction  $f$  of advected energy. Narayan & Yi (1995b) use detailed numerical methods to solve these equations at each radius  $r$  in order to determine the local properties of the flow and the spectrum that is produced. We obtain similar results with less effort analytically.

For the present analysis, the quantities of interest are the volume-integrated quantities,  $Q^+, Q^{e+}, Q^-$ , which are obtained by integrating  $q^+, q^{e+}, q^-$  throughout the volume of the advection region. Using scaled quantities, and the approximation  $H = R$ , the volume-integrated quantities are defined by

$$\begin{aligned} Q^X &= \int_{R_{\min}}^{R_{\max}} 4\pi R^2 q^X dR, \\ &= 3.23 \times 10^{17} m^3 \int_{r_{\min}}^{r_{\max}} q^X r^2 dr \text{ ergs s}^{-1}, \end{aligned} \quad (7)$$

where  $X$  denotes any quantity of interest. The lower limit is taken to be  $r_{\min} = 3$  since the self-similar solutions break down for  $r \lesssim \text{few}$  (Mastsumoto, Katao, & Fukue 1985; Narayan 1996). This choice of  $r_{\min}$  is also in accordance with previous calculations (see, e.g., Narayan et al. 1995; Lasota et al. 1996), and we find that this reproduces the detailed spectra quite well. To determine the upper limit, we use some of the properties of the flow developed by Narayan & Yi (1995b). Narayan & Yi (1995b) have shown that for  $r \gtrsim 10^3$ , the flow becomes a cool  $\sim 10^{8.5}$  K one-temperature plasma, and not much radiation is produced, while for  $r < 10^3$ , the electron temperature is fairly constant while the ion temperature increases as  $1/r$ . Since most of the radiation from these flows originates at  $r < 10^3$ , where  $T_e \gtrsim 10^9$ , and since the present discussion is interested in the radiation produced from such a flow, we set  $r_{\max} = 10^3$ . In the discussion that follows, we assume that the electron temperature is constant for  $r < 10^3$ , as suggested by the detailed calculations of Narayan & Yi (1995b). The energy balance equations take the form

$$\begin{aligned} Q^+ &= Q^{\text{adv}} + Q^{e+}, \\ Q^{e+} &= Q^{ie} + \delta Q^+, \\ Q^{e+} &= Q^-, \\ Q^- &= P_{\text{synch}} + P_{\text{Compton}} + P_{\text{brems}}, \end{aligned} \quad (8)$$

where  $P_{\text{synch}}, P_{\text{Compton}}, P_{\text{brems}}$  are the total cooling rates for the individual processes. The energy equations for the ions and electrons are solved self-consistently to determine the fraction of the advected energy  $f$  and the electron temperature  $T_e$ . To do this, we first give analytic equations for the heating terms  $Q^+, Q^{ie}$ , and in the next section determine the cooling terms  $P_{\text{synch}}, P_{\text{Compton}}, P_{\text{brems}}$ , and the spectra they produce.

### 3.1. Heating Processes: Ion Heating

The ions are heated by viscous forces. The total heating rate,  $Q^+$ , is obtained by using equation (7) and integrating  $q^+$ , as defined in Narayan & Yi (1995b), throughout the advection region. This gives

$$Q^+ = 9.39 \times 10^{38} \frac{1-\beta}{f} c_3 \dot{m} r_{\min}^{-1} \text{ ergs s}^{-1}, \quad (9)$$

where we have set  $r_{\max} \gg r_{\min}$ . For low values of  $\alpha$ ,  $c_3$  is independent of  $\alpha$ , and equation (9) shows that for fixed  $m$  and  $\dot{m}$ , the heating rate depends only on the fraction of gas to magnetic pressure.

### 3.2. Heating Processes: Electron Heating

The electrons are heated by two processes: by viscous heating  $\delta Q^+$ , where an expression for  $Q^+$  has been derived above, and by a transfer of energy from the ions to electrons via Coulomb interactions. The heating rate per unit volume due to

TABLE 1  
 $\theta_e$  AND  $K_2(1/\theta_e)$

$T_9$	$\theta_e$	$g(\theta_e)$	$\theta_e^3 K_2(1/\theta_e)$
1.00 .....	0.1686	12.003	8.783E-06
1.50 .....	0.2530	6.7292	2.982E-04
2.00 .....	0.3373	4.5134	2.472E-03
2.50 .....	0.4216	3.3386	1.092E-02
3.00 .....	0.5059	2.6261	3.408E-02
3.50 .....	0.5902	2.1540	8.550E-02
4.00 .....	0.6746	1.8209	1.849E-01
4.50 .....	0.7589	1.5746	3.593E-01
5.00 .....	0.8432	1.3859	6.438E-01
5.50 .....	0.9275	1.2369	1.083E+00
6.00 .....	1.0118	1.1166	1.731E+00
6.50 .....	1.0961	1.0175	2.654E+00
7.00 .....	1.1805	0.9345	3.930E+00
7.50 .....	1.2648	0.8640	5.650E+00
8.00 .....	1.3491	0.8035	7.922E+00
8.50 .....	1.4334	0.7509	1.086E+01
9.00 .....	1.5177	0.7048	1.462E+01
9.50 .....	1.6021	0.6641	1.933E+01
10.00 .....	1.6864	0.6278	2.519E+01

Coulomb interactions is given by Stepney & Guilbert (1983) and Narayan & Yi (1995b) and can be approximated to (see Appendix A.)

$$q^{\text{ie}} \simeq 5.61 \times 10^{-32} (T_i - T_e) b_1^2 m^{-2} \dot{m}^2 r^{-1} g(\theta_e) \text{ ergs cm}^{-3} \text{ s}^{-1}, \quad (10)$$

where we have substituted for  $n_e$ ,  $\theta_e = kT_e/m_e c^2$ , and

$$g(\theta_e) \equiv \frac{1}{K_2(1/\theta_e)} \left( 2 + 2\theta_e + \frac{1}{\theta_e} \right) e^{-1/\theta_e}, \quad (11)$$

which is tabulated for various values of temperature in Table 1. From Narayan & Yi (1995b), the ion temperature can be approximated to

$$T_i = 6.66 \times 10^{12} \beta c_3 r^{-1} - 1.08 T_e, \\ \simeq h r^{-1}, \quad (12)$$

where

$$h = 6.66 \times 10^{12} \beta c_3.$$

The second term in equation (12) has been neglected compared with the first since the electron temperatures are considerably lower than the ion temperatures for  $r \lesssim 10^3$ .

The total ion-electron heating rate for the electrons is (see eq. [7])

$$Q^{\text{ie}} \simeq 1.2 \times 10^{38} g(\theta_e) \alpha^{-2} c_1^{-2} c_3 \beta \dot{m} \dot{m}^2 r_{\text{min}}^{-1} \text{ ergs s}^{-1}, \quad (13)$$

where we have substituted for  $b_1$ ,  $h$ , and assumed  $r_{\text{max}} \gg r_{\text{min}}$ . Combining the equations above, the total heating of the electrons is given by

$$Q^{e+} = Q^{\text{ie}} + \delta Q^+, \\ \simeq 1.2 \times 10^{38} g(\theta_e) \alpha^{-2} c_1^{-2} c_3 \beta \dot{m} \dot{m}^2 r_{\text{min}}^{-1} + \delta 9.39 \times 10^{38} \left( \frac{1-\beta}{f} \right) c_3 \dot{m} \dot{m} r_{\text{min}}^{-1}. \quad (14)$$

The major source for electron heating depends on the value of  $\dot{m}$ ; for high  $\dot{m}$ ,  $Q^{\text{ie}} \gg \delta Q^+$ , whereas for low  $\dot{m}$ ,  $\delta Q^+ \gg Q^{\text{ie}}$ . By setting  $Q^{\text{ie}} = \delta Q^+$ , we can determine the transition accretion rate:

$$\dot{m} \sim 8.8 \times 10^{-5} \left( \frac{\alpha}{0.3} \right)^2 \left( \frac{\delta}{2000^{-1}} \right) \left( \frac{1-\beta}{0.5} \right) \left( \frac{\beta}{0.5} \right)^{-1} \left( \frac{c_1}{0.5} \right)^2 \left( \frac{f}{1.0} \right)^{-1} g(\theta_e)^{-1}. \quad (15)$$

#### 4. ENERGY BALANCE: COOLING PROCESSES AND THE COMPONENTS OF THE SPECTRUM

In order to balance the viscous and Coulomb heating, the electrons cool through three distinct processes: synchrotron, bremsstrahlung, and inverse-Compton emission. The emission in different regions of the spectrum is determined by these individual cooling processes. Synchrotron radiation is responsible for the radio to submillimeter emission, while a combination of bremsstrahlung emission and inverse-Compton scattering of synchrotron photons is responsible for the submillimeter to X-ray emission. This is one of the successes of the advection-dominated models: explaining, using few free parameters, the entire spectra of accreting systems. A natural question to ask is how does the amount of emission and shape of the final spectrum depend on variables like  $\alpha$ ,  $\beta$ ,  $m$ ,  $\dot{m}$ , and  $T_e$ ? Previous papers (see, e.g., Narayan & Yi 1995b; Narayan et al.

1996a) have used detailed numerical calculations to evaluate the spectrum produced. The analysis presented here gives less detailed spectra but is much faster in determining the general characteristics and the individual components of the spectra produced.

In the analysis that follows, the spectrum is divided into three components: the cyclosynchrotron component, and the bremsstrahlung and the inverse-Compton component. Figure 1 shows representative plots of the spectrum for a fixed mass  $m = 5 \times 10^9$ , and for different accretion rates  $\dot{m} = (3, 6, 12, 24) \times 10^{-4}$ , with  $\alpha = 0.3$ , and  $\beta = 0.5$ . For one curve, the individual components of the spectrum have been labeled as S for synchrotron, B for bremsstrahlung, and C for Comptonization. In the subsections below, each of these components is described with the appropriate analytic approximations.

#### 4.1. Cyclosynchrotron Emission and the Radio-Submillimeter Spectrum

The radio to submillimeter spectrum is defined by three quantities: (1) the luminosity of the radio spectrum, (2) the maximum (peak) frequency beyond which the spectrum falls off exponentially, and (3) the slope of the radio spectrum. We treat each of these separately.

In the optically thin limit, the spectrum of cyclosynchrotron radiation by an isotropic distribution of relativistic thermal electrons is given by (Mahadevan, Narayan, & Yi 1996; Narayan & Yi 1995b)

$$\epsilon_{\text{synch}} dv = 4.43 \times 10^{-30} \frac{4\pi n_e v}{K_2(1/\theta_e)} M(x_M), \quad (16)$$

where we use the extreme relativistic expression for  $M(x_M)$  given by

$$M(x_M) = \frac{4.0505}{x_M^{1/6}} \left( 1 + \frac{0.40}{x_M^{1/4}} + \frac{0.5316}{x_M^{1/2}} \right) \exp(-1.8899 x_M^{1/3}), \quad (17)$$

and

$$x_M \equiv \frac{2\nu}{3v_b \theta_e^2}, \quad v_b \equiv \frac{eB}{2\pi m_e c}. \quad (18)$$

The cyclosynchrotron photons in these plasmas are self-absorbed and give a blackbody spectrum, up to a critical frequency  $\nu_c$ . The frequency at which this occurs, at each radius  $r$ , is determined by evaluating the total cyclosynchrotron emission over

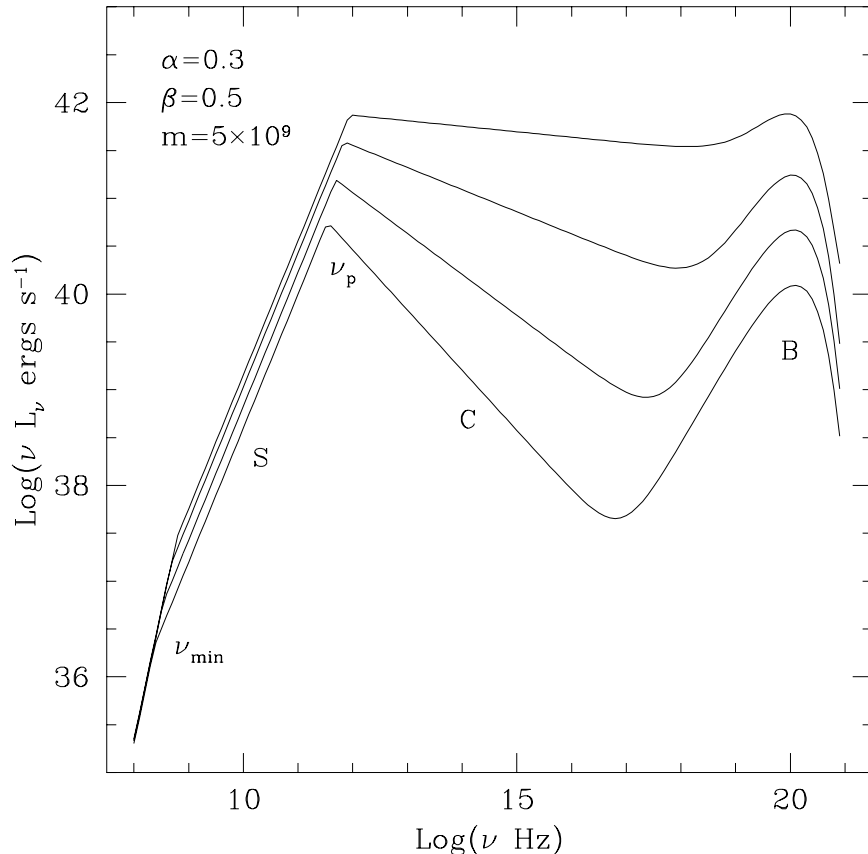


FIG. 1.—Spectrum produced by an advection-dominated disk with  $\alpha = 0.3$ ,  $\beta = 0.5$ ,  $m = 5 \times 10^9$ , and  $\dot{m} = (3, 6, 12, 24) \times 10^{-4}$ . The plots are calculated numerically by the method described in § 5.1.1. The three labels correspond to the three cooling processes: synchrotron cooling (S), Compton cooling (C), and bremsstrahlung cooling (B).  $\nu_p$  and  $\nu_{\min}$  correspond to the radio frequencies from the region  $3 \leq r \leq 10^3$ .

a volume of radius  $r$  and equating it to the Rayleigh-Jeans blackbody emission from the surface of this sphere. This gives the condition

$$4.43 \times 10^{-30} \frac{4\pi n_e v_c}{K_2(1/\theta_e)} M(x_M) \frac{4\pi}{3} R^3 = \pi 2 \frac{v_c^2}{c^2} k T_e 4\pi R^2, \quad (19)$$

which can be rewritten in terms of  $x_M$  as

$$\exp(1.8899 x_M^{1/3}) = 2.49 \times 10^{-10} \frac{4\pi n_e R}{B} \frac{1}{\theta_e^3 K_2(1/\theta_e)} \left( \frac{1}{x_M^{7/6}} + \frac{0.40}{X_M^{17/12}} + \frac{0.5316}{x_M^{5/3}} \right). \quad (20)$$

$x_M$  is determined in Appendix B. Given  $x_M$ , the cutoff frequency at each radius is determined by equation (18) to be

$$\begin{aligned} v_c &= 3/2 \theta_e^2 v_b x_M, \\ &= s_1 s_2 m^{-1/2} \dot{m}^{1/2} T_e^2 r^{-5/4} \text{ Hz}, \end{aligned} \quad (21)$$

where  $s_1$  is given in equations (5) and

$$s_2 \equiv 1.19 \times 10^{-13} x_M. \quad (22)$$

At this frequency, the radiation becomes optically thin, and the luminosity is given by the Rayleigh-Jeans part of the blackbody spectrum

$$\begin{aligned} L_{v_c} &= \pi 2 \frac{v_c^2}{c^2} k T_e 4\pi R^2, \\ &= s_3 T_e v_c^2 m^2 r^2 \text{ ergs s}^{-1} \text{ Hz}^{-1}, \quad s_3 = 1.05 \times 10^{-24}. \end{aligned} \quad (23)$$

This determines the luminosity at each point along the radio spectrum.

For a fixed  $T_e$ , equation (21) shows how the cutoff frequency varies with  $r$ . Emission observed at higher frequencies originates at smaller radii, closer to the central black hole. The peak frequency, and the power at that frequency are determined by setting  $r = r_{\min}$  in equations (21) and (23),

$$\begin{aligned} v_p &= s_1 s_2 m^{-1/2} \dot{m}^{1/2} T_e^2 r_{\min}^{-5/4} \text{ Hz}, \\ v_p L_{v_p} &= s_1^3 s_2^3 s_3 r_{\min}^{-7/4} m^{1/2} \dot{m}^{3/2} T_e^7 \text{ ergs s}^{-1}, \end{aligned} \quad (24)$$

which shows that the luminosity at the peak frequency is very sensitive to the electron temperature.

The slope of the radio spectrum is a direct consequence of  $x_M$  and  $T_e$  being essentially constant, and the Rayleigh-Jeans part of the blackbody spectrum. Since  $B \propto r^{-5/4}$ , equation (21) shows that  $r \propto v_c^{-4/5}$ . From equation (23),  $L_v \propto v_c^2 r^2 \propto v_c^{2/5}$ . The complete spectrum is obtained by rewriting equation (21) in terms of  $r$  and substituting in equation (23) to give

$$L_v \simeq s_3 (s_1 s_2)^{8/5} m^{6/5} \dot{m}^{4/5} T_e^{21/5} v^{2/5} \text{ ergs s}^{-1} \text{ Hz}^{-1}. \quad (25)$$

This produces a spectrum with slope of 2/5, which is similar to the slope of 1/3 produced by optically thin synchrotron emission (the dependence of  $x_M$  on  $r$  is not taken into account here, numerically,  $x_M \sim r^{1/15}$ , which makes  $L_v$  even closer to  $\sim v^{1/3}$ ). The advection-dominated models therefore give a very natural explanation to the characteristic 1/3 radio spectral indices observed when looking at putative black hole systems (Wrobel 1991; Slee et al. 1994; Narayan et al. 1995). The 2/5 spectral slope extends from  $v_p$  down to  $v_{\min}$ , where  $v_{\min}$  is the cutoff frequency given by setting  $r = r_{\max}$  in equation (21) (see Fig. 1). This is a direct consequence of the advection flows having a constant electron temperature for  $r \lesssim 10^3$ . Beyond this radius, the advection flows become a one-temperature plasma and  $T_e \propto r^{-1}$ , which gives a steeper radio slope of 22/13, as long as  $T_e \gtrsim 10^8 \text{ K}$  (below this temperature, there is no synchrotron radiation).

We assume that  $v_{\min} \ll v_p$  and obtain the total power from

$$\begin{aligned} P_{\text{synch}} &= \int_0^{v_p} L_v dv \simeq 0.71 v_p L_{v_p}, \\ &\simeq 5.3 \times 10^{35} \left( \frac{x_M}{1000} \right)^3 \left( \frac{\alpha}{0.3} \right)^{-3/2} \left( \frac{1-\beta}{0.5} \right)^{3/2} \left( \frac{c_1}{0.5} \right)^{-3/2} \left( \frac{c_3}{0.3} \right)^{3/2} \left( \frac{r_{\min}}{3} \right)^{-7/4} \left( \frac{T_e}{10^9} \right)^7 m^{1/2} \dot{m}^{3/2} \text{ ergs s}^{-1}. \end{aligned} \quad (26)$$

In this simple description, the synchrotron spectrum is assumed to terminate at  $v_p$  (cf. Fig. 1) and does not reproduce the exponential decay in the emission that is expected from thermal plasmas (Mahadevan et al. 1996). This is because, in this simple discussion, we have assumed that all the photons to be Comptonized occur at the peak frequency (see below), and so the Comptonized spectrum begins at  $v_p$ .

#### 4.2. Bremsstrahlung Emission: The Submillimeter Hard X-ray Spectrum

Bremsstrahlung emission is characterized by a constant luminosity  $L_v$ , up to a frequency  $h_v = k T_e$ , where the spectrum turns and falls off exponentially (see Fig. 1). The total emission due to bremsstrahlung radiation is given by equation (7) with  $q^X = q_{\text{brems}}$ , where  $q_{\text{brems}}$  is the bremsstrahlung emission per unit volume due to both electron-electron and electron-ion interactions. The bremsstrahlung emission per unit volume is given by Svensson (1982) (see also Stepney & Guilbert 1983;

Narayan & Yi 1995b),

$$q_{\text{brems}} = q_{\text{ei}} + q_{\text{ee}},$$

$$\simeq 1.48 \times 10^{-22} n_e^2 F(\theta_e) \text{ ergs cm}^{-3} \text{ s}^{-1}, \quad (27)$$

which represent the contributions from electron–electron and electron–ion interactions, and

$$F(\theta_e) = \begin{cases} 4 \left( \frac{2\theta_e}{\pi^3} \right)^{1/2} (1 + 1.781\theta_e^{1.34}) + 1.73\theta_e^{3/2} (1 + 1.1\theta_e + \theta_e^2 - 1.25\theta_e^{5/2}), & \theta_e < 1, \\ \left( \frac{9\theta_e}{2\pi} \right) [\ln(1.123\theta_e + 0.48) + 1.5] + 2.30\theta_e (\ln 1.123\theta_e + 1.28), & \theta_e > 1, \end{cases} \quad (28)$$

Using the expression for the number density, the total bremsstrahlung power is

$$P_{\text{brems}} = 4.78 \times 10^{34} \alpha^{-2} c_1^{-2} \ln(r_{\text{max}}/r_{\text{min}}) F(\theta_e) m \dot{m}^2, \quad (29)$$

and the spectrum due to bremsstrahlung emission is

$$L_{\text{brems}}(\nu) \simeq 2.29 \times 10^{24} \alpha^{-2} c_1^{-2} \ln(r_{\text{max}}/r_{\text{min}}) F(\theta_e) T_e^{-1} e^{-h\nu/kT_e} m \dot{m}^2 \text{ ergs s}^{-1} \text{ Hz}^{-1}, \quad (30)$$

which is shown in Figure 1. Comparing equation (29) with equation (26) shows that for most cases of interest,  $P_{\text{brems}} < P_{\text{synch}}$  and can be neglected when considering the total cooling rate of the flow. However, when considering the entire emission spectrum, bremsstrahlung emission is important since it contributes to the X-ray emission.

#### 4.3. Comptonization: The Submillimeter to Hard X-Ray Spectrum

In this discussion, we neglect the Comptonization of bremsstrahlung emission and only consider the Comptonization of the soft cyclosynchrotron photons. This is the other process responsible for the submillimeter to hard X-ray spectrum. The spectrum is defined by three quantities: (1) the initial frequency of the photons that are Comptonized, (2) the maximum final frequency of a Comptonized photon, and (3) the slope,  $\alpha_c$ , of the Comptonized spectrum (see Fig. 1).

The photons that are Comptonized are the soft cyclosynchrotron photons in the radio spectrum. The emission in the radio spectrum mainly occurs at the peak frequency,  $\nu_p$ , and so we can make the approximation that all the synchrotron photons to be Comptonized have an initial frequency of  $\nu_p$ . The maximum final frequency of a comptonized photon is  $h\nu_f = 3kT_e$ , which is the average energy of a photon for saturated comptonization in the Wien regime.

The optical depth to electron scattering,  $\tau_{\text{es}}$ , and how much a photon is amplified in one scattering, are the two quantities that determine the slope of the Compton spectrum. Photons at different radii see different optical depths, with photons at small radii seeing large optical depths and those at large radii seeing small optical depths. In this simple treatment we expect, on the average, that all the photons would probably see one-half the total optical depth. We therefore, take the optical depth to electron scattering to be one-half of that as given in Narayan & Yi (1995b),

$$\tau_{\text{es}} = 6.2 \alpha^{-1} c_1^{-1} \dot{m} r^{-1/2},$$

$$= (23.87 \dot{m}) \left( \frac{\alpha}{0.3} \right)^{-1} \left( \frac{c_1}{0.5} \right)^{-1} \left( \frac{r_{\text{min}}}{3} \right)^{-1/2}. \quad (31)$$

We find that this choice of  $\tau_{\text{es}}$  reproduces the more detailed Comptonized spectrum quite well (R. Narayan, private communication).

In the standard treatment of Comptonization (see, e.g., Rybicki & Lightman 1979, Dermer, Liang, & Canfield 1991), a photon with initial energy  $\epsilon_i$  that undergoes  $k$  scatterings has final energy  $\epsilon_f \simeq A^k \epsilon_i$ , where  $A$  is the mean amplification factor in one scattering which for a thermal plasma is

$$A = 1 + 4\theta_e + 16\theta_e^2. \quad (32)$$

For temperature ranges of interest,  $2 < A < 50$ . The luminosity of the emerging photons at frequency  $\nu_f$  has the power-law shape

$$L_{\nu_f} \simeq L_{\nu_i} \left( \frac{\nu_f}{\nu_i} \right)^{-\alpha_c}, \quad (33)$$

where

$$\alpha_c \equiv \frac{-\ln \tau_{\text{es}}}{\ln A}. \quad (34)$$

The total Compton power is

$$P_{\text{Compton}} = \int_{\nu_p}^{3kT_e/h} L_{\nu_f} d\nu_f,$$

$$= \frac{\nu_p L_{\nu_p}}{1 - \alpha_c} \left\{ \left[ \frac{6.2 \times 10^7 (T_e/10^9)}{(\nu_p/10^{12})} \right]^{1-\alpha_c} - 1 \right\} \text{ ergs s}^{-1}. \quad (35)$$

Equations (33), (34), and (35) show how the Compton power depends on the optical depth and temperature through the slope of the spectrum  $\alpha_c$ . If  $\alpha_c \gg 1$ , Comptonization can be neglected. If  $\alpha_c \lesssim 1$ , then there is significant comptonization of the cyclosynchrotron photons, and the cooling is dominated by the inverse-Compton losses. The actual determination of  $\alpha_c$  is done self-consistently and is discussed in § 5. Although equation (35) is used to determine the total Compton power in the subsequent sections (see § 5), it is instructive to analytically approximate equation (35) for  $\alpha_c \gg 1$ , and  $\alpha_c < 1$ , to determine how the Compton power scales in these regimes. We consider these two cases below and show how the value of  $\alpha_c$  determines whether the Comptonization of the soft cyclosynchrotron photons dominates over bremsstrahlung emission in the submillimeter to X-ray region of the spectrum.

#### 4.3.1. $\alpha_c > 1$ : Low Compton Cooling

For  $\alpha_c > 1$ , the first term in the curly braces in equation (35) can be neglected which gives

$$P_{\text{Compton}}(\alpha_c > 1) \simeq \frac{\nu_p L_{\nu_p}}{\alpha_c - 1}, \quad (36)$$

with  $\alpha_c \gg 1$  corresponding to no comptonization. Comparing this with equation (26), the total Compton power is proportional to the total synchrotron power. If  $\alpha_c \gg 1$ , then the Compton power is less than the synchrotron power and can be neglected when determining the total cooling rates. When  $1 < \alpha_c < 2$ , however, the Compton power is greater than the synchrotron power and contributes comparably to the total cooling rate.

#### 4.3.2. $\alpha_c < 1$ : Significant Compton Cooling

For  $\alpha_c < 1$ , the second term in curly braces in equation (35) can be neglected, which gives

$$P_{\text{Compton}}(\alpha_c < 1) \simeq \left[ \frac{6.2 \times 10^7 (T_e/10^9)}{\nu_p/10^{12}} \right]^{1-\alpha_c} \frac{\nu_p L_{\nu_p}}{1-\alpha_c}. \quad (37)$$

In this regime the Compton power dominates the total synchrotron power. The Compton power when  $\alpha_c = 1$  is obtained by taking the limit as  $\alpha_c \rightarrow 1$  of equation (35).

#### 4.3.3. Compton Luminosity

The luminosity in the submillimeter to X-rays due to Comptonization is

$$L_{\text{Compton}} \simeq \nu_p^{\alpha_c} L_{\text{synch}}(\nu_p) \nu^{-\alpha_c} \text{ ergs s}^{-1} \text{ Hz}^{-1} \quad (38)$$

and is sensitive to whether  $\alpha_c$  is less than, equal to, or greater than 1. For  $\alpha_c \gg 1$ , the bremsstrahlung luminosity in the submillimeter to X-rays is greater than the Compton luminosity. When  $\alpha_c < 1$ , Comptonization dominates the submillimeter to X-ray spectrum, and when  $1 < \alpha_c < 2$ , both bremsstrahlung and comptonization are dominant. Figure 1 shows how an increase in the accretion rate increases the slope of the Compton spectrum. At low  $\dot{m}$ , the bremsstrahlung emission dominates the X-ray emission, when  $\alpha_c > 1$ , whereas for high  $\dot{m}$ ,  $\alpha_c < 1$ , and the Comptonized spectrum dominates the X-ray emission.  $\alpha_c$  therefore determines the dominant source of emission at these frequencies. Note that in this simple description of Comptonization, the spectrum begins from  $\nu = \nu_p$  (see, Figure 1) and therefore does not reproduce the characteristic dip in the spectrum between radio and submillimeter wavelengths (see, e.g., Narayan et al. 1995). A more detailed Compton calculation would be needed for this.

### 5. GENERAL PROPERTIES OF THE FLOW

In the following sections, we use the results obtained to determine general properties of the advection-dominated flow. We first determine the temperature of the gas and  $\alpha_c$ , then the total luminosity from the flow, and finally the critical accretion rate  $\dot{m}_{\text{crit}}$  above which the advection solution does not exist.

#### 5.1. Equilibrium Temperatures and $\alpha_c$

Since the electrons are responsible for cooling, the temperature in these flows is determined by the energy balance equation for the electrons. The sum of the individual cooling processes is equated to the total heating of the electrons, and this equation is solved self-consistently for the temperature. We first determine the equilibrium temperature and  $\alpha_c$  through simple numerical methods and then provide analytic approximations which determine them.

##### 5.1.1. Numerical Method

For a given  $m$ ,  $\dot{m}$ ,  $\alpha$ , and  $\beta$ , the total heating of the electrons is equated to the individual cooling processes,  $Q^{e+} = P_{\text{synch}} + P_{\text{brems}} + P_{\text{Compton}}$ , and the electron temperature is varied until this equality is satisfied. At each value of  $T_e$ , the slope of the Comptonized spectrum is determined through equation (34). Solving for the electron temperature therefore fixes the slope of the Comptonized spectrum. Figure 2 shows numerical plots of the equilibrium temperature as a function of  $\dot{m}$  for different values of the black hole mass  $m$ . Here,  $\alpha = 0.3$ ,  $\beta = 0.5$ , and  $\delta = 1/2000$ . The corresponding values of  $x_M$  at each  $\dot{m}$  is also shown. At high  $\dot{m}$ , the equilibrium temperatures are independent of  $m$  and are constant at a value  $T_e \simeq 2.0 \times 10^9$ . Further, at low  $\dot{m}$ ,  $T_e$  increases with decreasing  $\dot{m}$ . Note, however, that if  $\delta = 0$ , then equation (C4) shows that the temperature decreases as  $\dot{m}$  decreases. This is because synchrotron cooling is the dominant source of cooling and is much more efficient than the Coulomb heating at low  $\dot{m}$ .

Figure 3 shows the value of  $1 - \alpha_c$ , the slope of the spectrum on a  $\nu L_\nu$  plot, as a function of  $\dot{m}$ , for different values of the central mass  $m$ . These correspond to the equilibrium conditions as shown in Figure 2. At low  $\dot{m}$ ,  $\alpha_c$  becomes constant, which is



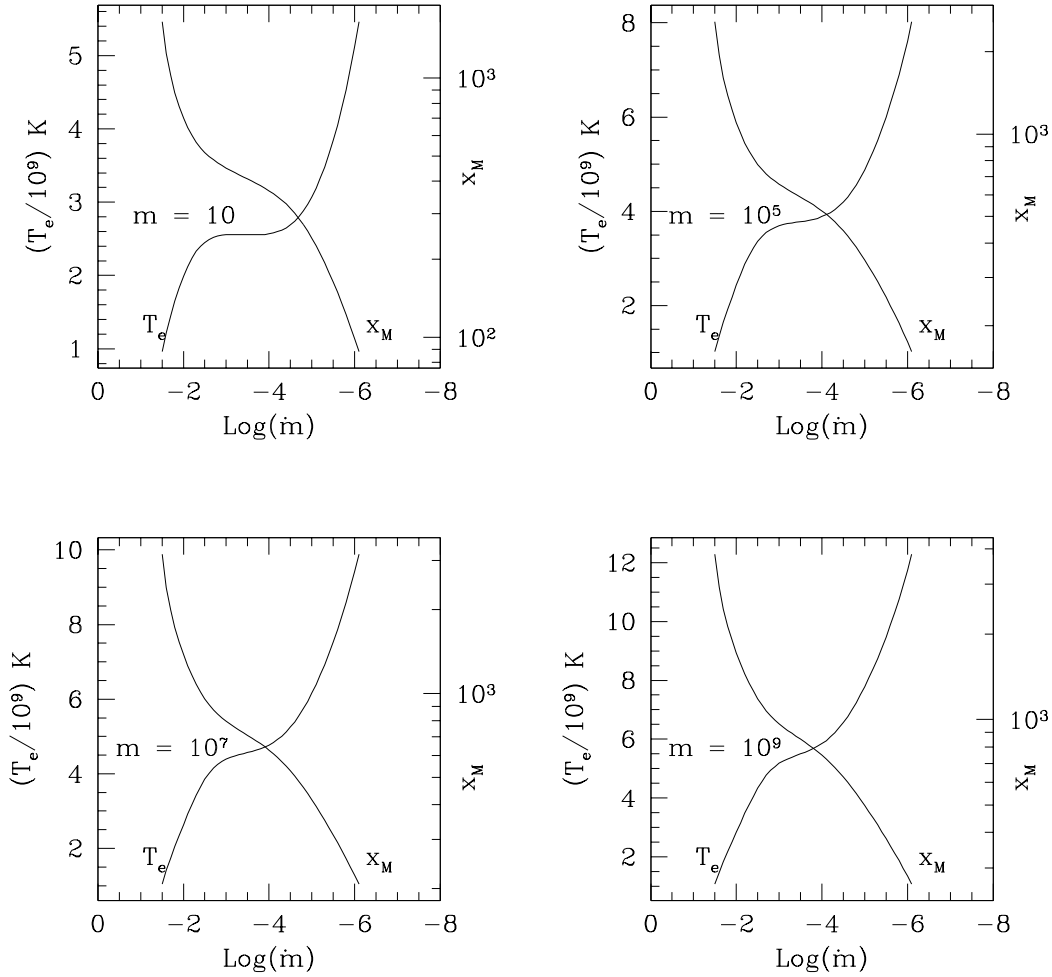


FIG. 2.—Equilibrium temperatures as a function of  $\dot{m}$ , for different values of  $m$ , and the corresponding values of  $x_M$ . For low  $\dot{m}$ ,  $\delta Q^+$  dominates the heating of the electrons.

expected since both  $\ln A$ ,  $\ln \tau_{\text{es}} \propto \ln \dot{m}$ . The value of this constant depends on the mass of the central black hole. At high accretion rates,  $\alpha_c \sim 0.5$ .

#### 5.1.2. Analytic Determination

An analytic determination of the equilibrium electron temperature allows an understanding of how it scales with different quantities in these models. To simplify the equations that follow, note that equations (26), (29), and (35) show that  $P_{\text{brems}} < P_{\text{synch}}$  and that depending on the value of  $\alpha_c$ ,  $P_{\text{synch}}$  can be greater or less than  $P_{\text{Compton}}$ . Further, since  $P_{\text{brems}}$  is very insensitive to the electron temperature [ $\propto F(\theta_e)$ ], as compared with  $(P_{\text{synch}} + P_{\text{Compton}} \propto T_e^7)$ , we find that for all ranges of  $m$ ,  $\dot{m}$ , the contribution to the total cooling by bremsstrahlung emission, is negligible compared with synchrotron and Compton cooling, at the equilibrium temperatures. We therefore neglect bremsstrahlung cooling in the analysis that follows.

A rough estimate of  $\alpha_c$ , for a given  $\dot{m}$ , can be obtained from equation (31) and (34). Using the range of temperatures of interest ( $10^9 \leq T_e \leq 2 \times 10^{10}$ ) to determine the maximum and minimum values of  $\ln A$ , and setting  $\alpha_c = 1$ , equations (34) and (31) show that if  $\dot{m} \lesssim 10^{-4}\alpha$ , then  $\alpha_c \gtrsim 1$ , and if  $\dot{m} \geq 3 \times 10^{-3}\alpha$ , then  $\alpha_c \leq 1$ . However, for  $10^{-4}\alpha \leq \dot{m} \leq 10^{-2}\alpha$ , the value of  $\alpha_c$  can be either greater or less than 1, depending on the temperature that has to be solved self-consistently. We consider the two cases.

$\alpha_c > 1$ .—In this limit, synchrotron and Compton emission are the dominant sources of cooling, and depending on the value of  $\alpha_c$  Compton cooling is comparable to or less than the total synchrotron cooling (see § 4.3.1). Bremsstrahlung cooling is neglected. The total cooling rate is given by

$$\begin{aligned} Q^- &\simeq \left(0.71 + \frac{1}{\alpha_c - 1}\right) v_p L_{v_p} \\ &\simeq A_c v_p L_{v_p}, \end{aligned} \quad (39)$$

where the first term is due to synchrotron cooling and the second is due to Compton cooling (for  $\alpha_c \gg 1$ , we only consider synchrotron cooling and  $A_c = 0.71$ ). This has to be equal to the total heating  $Q^{e+}$ . However when  $\alpha_c > 1$  and  $\dot{m} < 10^{-3}\alpha^2$ , from equation (15), this is when  $Q^{\text{ic}}$  can be neglected compared with  $\delta Q^+$  (see Appendix C for the case  $\delta = 0$ ). Setting

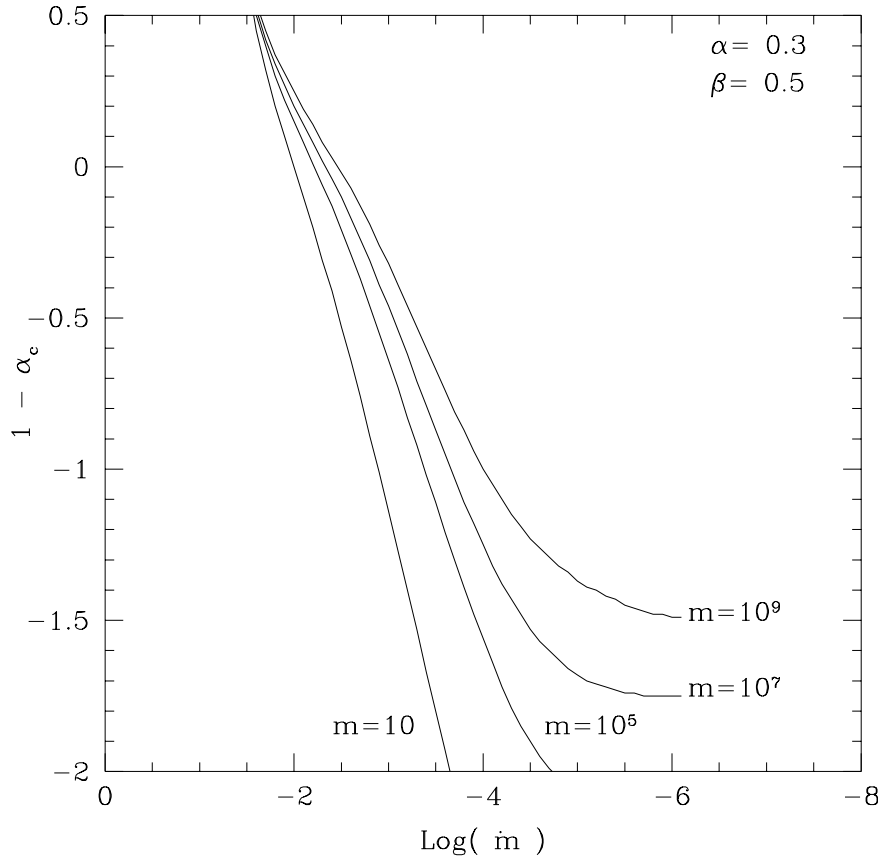


FIG. 3.—Plot of  $1 - \alpha_c$  as a function of  $\dot{m}$  for the corresponding plots in Fig. 2

$\delta Q^+ = Q^-$  and rearranging terms gives

$$T_e = \frac{1.1 \times 10^9}{A_c^{1/7}} \left( \frac{\delta}{2000^{-1}} \right)^{1/7} \left( \frac{x_M}{300} \right)^{-3/7} \left( \frac{\alpha}{0.3} \right)^{3/14} \left( \frac{1-\beta}{0.5} \right)^{-1/14} \left( \frac{c_1}{0.5} \right)^{3/14} \left( \frac{c_3}{0.3} \right)^{-1/14} \left( \frac{r_{\min}}{3} \right)^{3/28} \dot{m}^{1/14} \dot{m}^{-1/14} \text{ K}, \quad (40)$$

where  $A_c^{1/7}$  varies from 0.95 to 1.4, and we have scaled  $x_M$  appropriately for low  $\dot{m}$  (see Fig. 2). Figure 2 shows the temperature increasing faster with  $\dot{m}$  than indicated above. This is mainly due to the sensitivity of the temperature on  $x_M$ , which decreases since the synchrotron emission decreases as  $\dot{m}^2$ . However, comparing the four panels in Figure 2 shows that the temperature is fairly insensitive to the mass of the central black hole.

$\alpha_c < 1$ .—In this regime we find simple recursive formulae that can be used to determine  $T_e$  analytically. For  $\alpha_c < 1$ , both synchrotron and bremsstrahlung cooling is negligible, and the total cooling,  $Q^-$ , is given by equation (35)

$$\begin{aligned} Q^- &\simeq P_{\text{Compton}} = \frac{v_p L_{v_p}}{1 - \alpha_c} \left\{ \left[ \frac{6.2 \times 10^7 (T_e/10^9)}{(v_p/10^{12})} \right]^{1-\alpha_c} - 1 \right\}, \\ &\equiv \frac{v_p L_{v_p}}{1 - \alpha_c} (C_F^{1-\alpha_c} - 1), \end{aligned} \quad (41)$$

where the Compton factor  $C_F$  has been defined for convenience. When  $\alpha_c < 1$ ,  $\dot{m} \gtrsim 10^{-3} \alpha$ , and from equation (15)  $\delta Q^+$  is negligible with  $Q^{\text{ie}}$ . Therefore,  $Q^{e+} \simeq Q^{\text{ie}}$ . Instead of equating  $Q^{\text{ie}}$  to  $P_{\text{Compton}}$  and solving for the temperature, a good approximation to the temperature can be obtained by rewriting equation (34) as a quadratic,

$$1 + 4\theta_e + 16\theta_e^2 = \tau_{\text{es}}^{-1/\alpha_c}, \quad (42)$$

which gives

$$\left( \frac{T_e}{10^9} \right) = 0.744 [ (4\tau_{\text{es}}^{-1/\alpha_c} - 3)^{1/2} - 1 ]. \quad (43)$$

Since  $0.5 \leq \alpha_c \leq 1.0$  for all cases of interest, we can get an idea for the range of temperatures possible for a given  $\dot{m}$  by setting  $\alpha_c = 0.5$  and  $\alpha_c = 1.0$  (lower values of  $\alpha_c$  would require very high  $\dot{m}$ , and this is where the advection solutions are no longer valid). This gives

$$2.15 \times 10^8 \dot{m}^{-1/2} \lesssim T_e \lesssim 3.12 \times 10^7 \dot{m}^{-1}. \quad (44)$$

For high  $\dot{m} \sim 10^{-2}$  systems in this regime, equation (44) indicates that the range of temperatures possible is confined to  $2.15 \times 10^9 \leq T_e \leq 3.12 \times 10^9$ , whether the systems are  $1M$  or  $10^9 M_\odot$  black holes (see Fig. 2). However, as  $\dot{m}$  decreases, while  $\alpha_c < 1$ , the temperature range possible increases (e.g., for  $\dot{m} \sim 10^{-2.5}$ ,  $3.8 \times 10^9 \leq T_e \leq 9.8 \times 10^9$ ), and a more accurate evaluation of  $\alpha_c$  is necessary.

We can determine, to a first approximation, the temperature in these systems by setting  $\alpha_c \sim 0.75$  in equation (43). From this estimate, a more accurate determination of  $\alpha_c$  can be obtained by equating  $Q^{\text{ie}}$  to equation (41) and rewriting to give

$$1 - \alpha_c = \log \left[ \frac{Q^{\text{ie}}}{v_p L_{vp}} (1 - \alpha_c) + 1 \right] / \log (C_F). \quad (45)$$

Since logarithms are slowly varying functions,  $\alpha_c$  in the logarithm can be set to  $\sim 0.75$ , as before, to obtain

$$1 - \alpha_c \simeq \log \left( \frac{Q^{\text{ie}}}{4v_p L_{vp}} - 1 \right) / \log (C_F), \quad (46)$$

where  $1 - \alpha_c$  is the slope of the spectrum on a  $v L_v$  plot,

$$\frac{Q^{\text{ie}}}{v_p L_{vp}} = 3.57 \times 10^2 \left( \frac{x_M}{1000} \right)^{-3} \left( \frac{\alpha}{0.3} \right)^{-1/2} \left( \frac{\beta}{0.5} \right) \left( \frac{1-\beta}{0.5} \right)^{-3/2} \left( \frac{c_1}{0.5} \right)^{-1/2} \left( \frac{c_3}{0.3} \right)^{-1/2} \left( \frac{r_{\min}}{3} \right)^{3/4} \left( \frac{T_e}{10^9} \right)^{-7} g(\theta_e) m^{1/2} \dot{m}^{1/2}, \quad (47)$$

and

$$C_F = 1.46 \times 10^3 \left( \frac{x_M}{1000} \right)^{-1} \left( \frac{\alpha}{0.3} \right)^{1/2} \left( \frac{1-\beta}{0.5} \right)^{-1/2} \left( \frac{c_1}{0.5} \right)^{1/2} \left( \frac{c_3}{0.3} \right)^{-1/2} \left( \frac{r_{\min}}{3} \right)^{5/4} \left( \frac{T_e}{10^9} \right)^{-1} m^{1/2} \dot{m}^{-1/2}. \quad (48)$$

Solving for  $\alpha_c$  then gives a better approximation for the temperature from equation (43). This process can be iterated for accurate determination of both  $T_e$  and  $\alpha_c$ , but we find that fairly accurate results are obtained without any iterations.

### 5.2. Total Luminosity

For a given accretion rate  $\dot{M}$ , and matter-to-energy conversion of  $\eta_{\text{eff}} = 0.1$ , standard accretion disks predict a total luminosity of  $L_{\text{disk}} \simeq \eta_{\text{eff}} \dot{M} c^2$ . Advection-dominated accretion produces a lower luminosity because most of the viscously dissipated energy is advected inward with the flow and deposited into the black hole instead of being radiated. The total luminosity from these disks is equal to the total energy being emitted by the various cooling processes,  $L_{\text{ADAF}} = Q^-$ . However, since  $Q^{e+} = Q^-$ , detailed knowledge of the cooling processes is not required here, and the total luminosity is simply  $L_{\text{ADAF}} = Q^{e+}$ .

Depending on the value of  $\dot{m}$ , the total heating of the electrons is either dominated by  $Q^{\text{ie}}$  or by  $\delta Q^+$ . The luminosities in both these regions are determined by setting  $L_{\text{ADAF}} = \max(Q^{\text{ie}}, \delta Q^+)$ . For  $\dot{m} > 10^{-3} \alpha^2$  (see eq. [15]),  $Q^{\text{ie}}$  dominates, and the total luminosity is given by

$$\begin{aligned} L_{\text{ADAF}} &\simeq 1.2 \times 10^{38} g(\theta_e) c_1^{-2} c_3 \beta r_{\min}^{-1} \alpha^{-2} m \dot{m}^2, \\ &\simeq \eta_{\text{eff}} \dot{M} c^2 \left[ 0.20 \left( \frac{\dot{m}}{\alpha^2} \right) g(\theta_e) \left( \frac{\beta}{0.5} \right) \left( \frac{c_1}{0.5} \right)^{-2} \left( \frac{c_3}{0.3} \right) \left( \frac{r_{\min}}{3} \right)^{-1} \right] \text{ergs s}^{-1}, \end{aligned} \quad (49)$$

where  $c$  is the speed of light. This also gives the luminosity for the case  $\delta = 0$ . For  $\dot{m} \lesssim 10^{-3} \alpha^2$ ,  $\delta Q^+$  dominates the electron heating, and the total luminosity can be written as

$$L_{\text{ADAF}} \simeq \eta_{\text{eff}} \dot{M} c^2 \left[ 2.0 \times 10^{-4} \left( \frac{\delta}{2000^{-1}} \right) \left( \frac{1-\beta}{0.5} \right) \left( \frac{c_3}{0.3} \right) \left( \frac{r_{\min}}{3} \right)^{-1} \left( \frac{f}{1.0} \right)^{-1} \right] \text{ergs s}^{-1}. \quad (50)$$

The factor in the square brackets is the factor by which the efficiency is reduced relative to the usual 10% from standard thin accretion disks. At high accretion rates, the luminosity decreases linearly with  $\dot{m}$ , but there is no additional  $\dot{m}$  dependence at low accretion rates since the ion-electron transfer rate becomes very inefficient, and the cooling processes have to compensate only for a fraction of the viscous heating generated. Using  $L_{\text{ADAF}} = Q^{e+}$  and the numerical method in § 5.1.1, Figure 4 shows plots of  $L_{\text{ADAF}}/L_{\text{Edd}}$  as a function of  $\dot{m}$  for various values of  $\alpha$ . Disks with high values of  $\alpha$  are more sub-Eddington in their luminosities than disks with low  $\alpha$ . At low  $\dot{m}$ , the luminosities are independent of  $\alpha$  (see eq. [50]). Although Figure 4 is calculated for  $m = 10^9$ , it can be used for any value of  $m$ , since the ratio  $L_{\text{ADAF}}/L_{\text{Edd}}$  is independent of  $m$ , and the equilibrium temperatures are fairly insensitive to the exact value of  $m$ .

### 5.3. Determining $\dot{m}_{\text{crit}}$

In advection flows where  $\dot{m} \ll 1$ , Narayan & Yi (1995b) have shown that  $f \simeq 1$ . However, as  $\dot{m}$  increases, the Coulomb interactions between the ions and electrons become more efficient, and more of the viscously generated energy is transferred from the ions to the electrons. This decreases the amount of energy that can be advected inwards with the flow, and the value of  $f$  therefore also decreases. As  $\dot{m}$  is increased further, the flow radiates the generated heat more efficiently, becomes less advection dominated, and becomes optically thick. Narayan & Yi (1995b) have shown that for  $\dot{m}$  greater than a critical value,

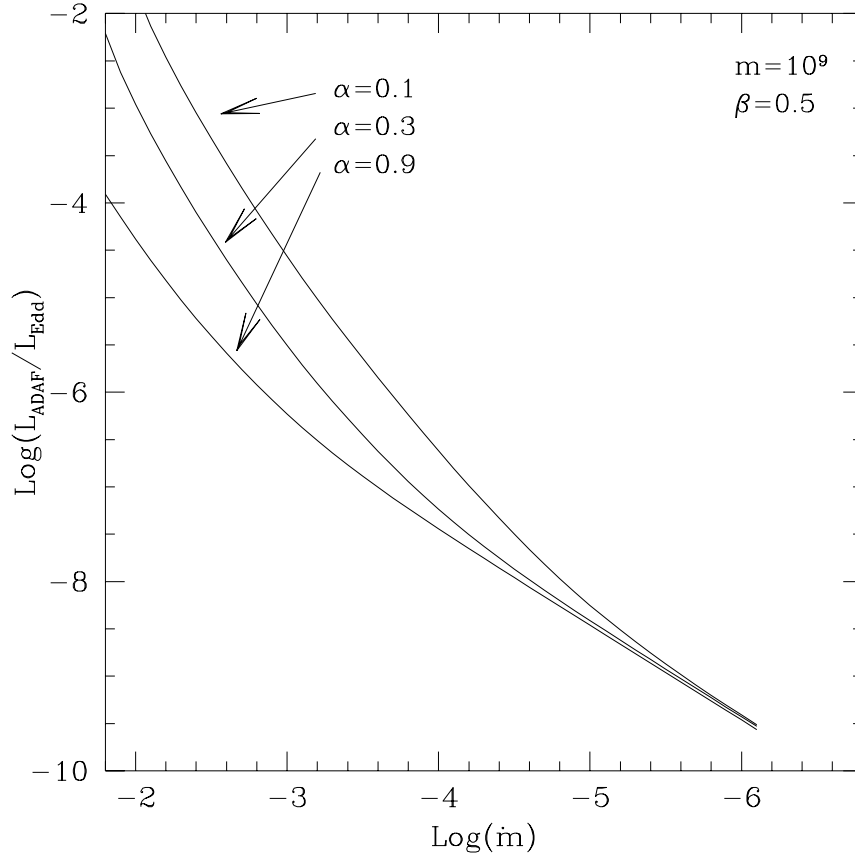


FIG. 4.—Plot of  $L_{\text{ADAF}}/L_{\text{Edd}}$  as a function of  $\dot{m}$  for different values of  $\alpha$ . The plot can be used for any value of  $m$  (see text).

$\dot{m}_{\text{crit}}$ , the energy equations (see eq. [8]) have no solution, and the advection-dominated solution ceases to exist. Here, we determine what  $\dot{m}_{\text{crit}}$  is, for a given set of parameters  $m, \alpha, \beta$ .

To determine the critical accretion rate, the energy equation becomes  $Q^+(1-f) = Q^- \simeq Q^{\text{ie}}$ , since  $Q^{\text{ie}} \gg \delta Q^+$  in this regime ( $\dot{m} \gg 10^{-3} \alpha^2$ ). Dividing equation (9) by equation (13) and rewriting in terms of  $\dot{m}$  gives

$$\dot{m} = 7.8 \frac{(1-f)}{f} \frac{(1-\beta)}{\beta} \alpha^2 c_1^2 \frac{1}{g(\theta_e)}. \quad (51)$$

When  $\dot{m} \sim \dot{m}_{\text{crit}}$ , we expect  $f \sim 0.5$ , which requires about half the generated energy to be radiated away, which is a reasonable assumption. Also, for very high  $\dot{m} \sim 10^{-1.7}$ , equation (44) shows that  $T_e \sim 1.5 \times 10^9$ , which gives  $g(\theta_e) \sim 7$ . Setting  $\beta = 0.5$ ,  $c_1 \simeq 0.5$ , gives

$$\dot{m}_{\text{crit}} \simeq 0.28 \alpha^2. \quad (52)$$

The critical accretion rate, in scaled units, is therefore independent of the mass of the accreting object but depends quite strongly on  $\alpha$ . This suggests a large value of  $\alpha \sim 1$  since a low value of  $\alpha \sim 0.01$  gives a very small  $\dot{m}_{\text{crit}}$ , which is not high enough to explain even moderate luminosities. Advection models that have had success in explaining black hole candidates (see, e.g., Lasota et al. 1996; Narayan et al. 1995) use  $\alpha \sim 0.1$ – $0.3$  and, as suggested by Narayan (1996), could be as high as  $\sim 1$  to explain low-luminosity AGNs.

## 6. DO ELLIPTICAL GALAXIES HOST DEAD QUASARS?

In this section we use the results above and apply them to a specific problem which was first suggested by Fabian & Canizares (1988). We give a brief introduction to the problem, derive the results of Fabian & Canizares (1988), and then, as suggested by Fabian & Rees (1995) show how advection-dominated accretion flows results resolve this problem.

### 6.1. Outline

Most nearby bright elliptical galaxies are believed to host “dead” or inactive quasars (Soltan 1982; Fabian & Canizares 1988; Fabian & Rees 1995). From energetic arguments or from the properties of broad-line-emitting regions, the masses of quasars are found to be between  $10^8$  and  $10^9 M_\odot$  (Wandel & Mushotzky 1986). We should therefore expect black hole masses of this size at the cores of bright elliptical galaxies and should be able to detect accretion of the ambient gas onto the central black hole.

From X-ray profiles of elliptical galaxies, we can determine the density and temperature of the gas within the central kiloparsec region. Since elliptical galaxies are thermally supported and are most likely to accrete spherically, we can use the

classical Bondi formula to obtain what is essentially a lower limit to the luminosity produced by a black hole of a given mass. Fabian & Canizares (1988) have looked at six bright nearby ellipticals and, from the observed X-ray luminosity of the gas, have determined upper limits for the black hole masses in these galaxies to be  $< 3 \times 10^7 M_\odot$ . This is in conflict with the expected masses, in these galaxies, as determined by Soltan (1982), together with the independent estimates of quasar masses as determined by Wandel & Mushotzky (1986). One of the conclusions is to reject the black hole hypothesis for quasars, since requiring higher mass black holes would lead to a higher luminosity in the X-rays, which is not observed. To reconcile these differences, Fabian & Rees (1995) have recently suggested that the massive black holes at the centers of these galaxies might be undergoing advection-dominated accretion that would help reconcile these differences.

### 6.2. Standard Accretion

In this section we show how Fabian & Canizares (1988) use standard Bondi accretion to deduce severe upper limits to the masses of the black holes at the centers of bright elliptical galaxies.

A lower limit on the accretion luminosity is obtained by assuming that the gas accretes spherically onto the central black hole by Bondi accretion. Following Fabian & Canizares (1988), the accretion radius, the radius at which the influence of gravity by the central black hole dominates the dynamics of the gas, is  $R_{\text{acc}} = \alpha_b GM/c_s^2 = 4.32\alpha_b M_8 T_7^{-1}$  pc, where  $c_s \simeq 10^4 T^{1/2}$  cm s $^{-1}$ , and  $\alpha_b$  is a factor including the ratio of specific heats (see Bondi 1952).  $\alpha_b > 0.5$  and is probably  $\sim 1$ . The Bondi accretion rate is given by  $\dot{M} = 1.86 \times 10^{-4} \alpha_b^2 P_6 T_7^{-5/2} M_8^2 M_\odot \text{ yr}^{-1}$ , where we have written  $P = n_e T = 10^6 P_6 \text{ cm}^{-3} \text{ K}$ , to keep the notation of Fabian & Canizares (1988). This gives a luminosity assuming a 10% matter-to-energy conversion, of

$$L_b = 1.06 \times 10^{42} \alpha_b^2 P_6 T_7^{-5/2} M_8^2 \text{ ergs s}^{-1}. \quad (53)$$

From equation (53), if  $P_6 = T_7 = 1$ , black hole masses of  $10^8$ – $10^9 M_\odot$  should be detectable.

$P_6$  and  $T_7$  can be determined by looking at the radial X-ray profiles of elliptical galaxies. Canizares, Fabbiano, & Trinchieri (1987) find the mean temperatures of the gas to be  $\sim 0.5$ – $4 \times 10^7$  K and determine the central number density by calculating the volume emissivity of the X-ray gas,  $\epsilon = 4\pi n_e(0)^2 a_X^2 [\ln(2R_X/a_X) - 1] \text{ cm}^{-3}$ , where  $a_X$  is the core radius, and  $R_X$  is the maximum radial extent of the gas, which is chosen to be  $50 a_X$ . (This choice is consistent with the radial profiles in Trinchieri, Fabbiano, & Canizares 1986.) Using the cooling function  $\Lambda(T) = 10^{-19} T^{-1/2} \text{ ergs cm}^{-3} \text{ s}^{-1}$ , the central density is

$$\begin{aligned} n_e(0) &= \left[ \frac{L_X}{\Lambda(T) 4\pi a_X^3 3.61} \right]^{1/2} \text{ cm}^{-3} \\ &= 4.88 \times 10^{-2} \left( \frac{L_X}{10^{41} \text{ ergs s}^{-1}} \right)^{1/2} \left( \frac{a_X}{1 \text{ kpc}} \right)^{-3/2} T_7^{1/4} \text{ cm}^{-3}. \end{aligned} \quad (54)$$

We assume that the central density  $n_e(0)$  evaluated continues on to the central black hole, i.e., there is no central cavity in these galaxies. Using  $P = n_e T$  in equation (53) the expected X-ray luminosity from accretion in terms of the total observed X-ray luminosity from the gas is given by

$$L_b = 5.17 \times 10^{41} \alpha_b^2 M_8^2 T_7^{1/4} (a^3 T_7^3)^{-1/2} \left( \frac{L_X}{10^{41}} \right)^{1/2} \text{ ergs s}^{-1}, \quad (55)$$

where  $a = (a_X/1 \text{ kpc})$ . This corresponds to an accretion rate in Eddington units of

$$\dot{m} = 4.16 \times 10^{-5} \alpha_b^2 M_8 T_7^{1/4} (a^3 T_7^3)^{-1/2} \left( \frac{L_X}{10^{41}} \right)^{1/2}. \quad (56)$$

Rewriting equation (55) to resemble Fabian & Canizares (1988) and setting  $\alpha_b = 0.5$ , we have

$$\frac{L_b}{L_X} = 1.3 M_8^2 \left[ \left( \frac{L_X}{10^{41}} \right) a^3 T_7^3 \right]^{-1/2} T_7^{1/4}. \quad (57)$$

The quantity  $L_b/L_X$  is a measured quantity which is obtained by using the X-ray profiles of the elliptical galaxies and taking the ratio of the X-ray emission from the central arcsecond region to the total X-ray gas emission from the whole galaxy. Table 2 shows the parameters used for three of the six galaxies analyzed by Fabian & Canizares (1988). These galaxies were chosen since they have good *Einstein* HRI data (Trinchieri et al. 1986). The core X-ray luminosities were estimated from the surface brightness profiles given in Trinchieri et al. (1986), taking into account the resolution of the detector. The best fits for the core

TABLE 2  
GALAXIES ANALYZED FROM FABIAN & CANIZARES (1988)

GALAXY (NGC)	DISTANCE (Mpc)	$M_B$	$a_X$ (kpc)	$T_7$	$\log(L_X)$	$L_b/L_X$	$10^8 M_\odot$	
							(FC)	(Advection)
4472.....	20	−22.8	0.48	1.4	41.71	0.025	0.14	6.7
4649.....	20	−22.2	0.96	1.4	41.40	0.047	0.29	24.1
4636.....	16.4	−21.6	1.18	1.2	41.64	0.030	0.27	14.6

NOTE.—Distances are taken from Trinchieri et al. 1986.

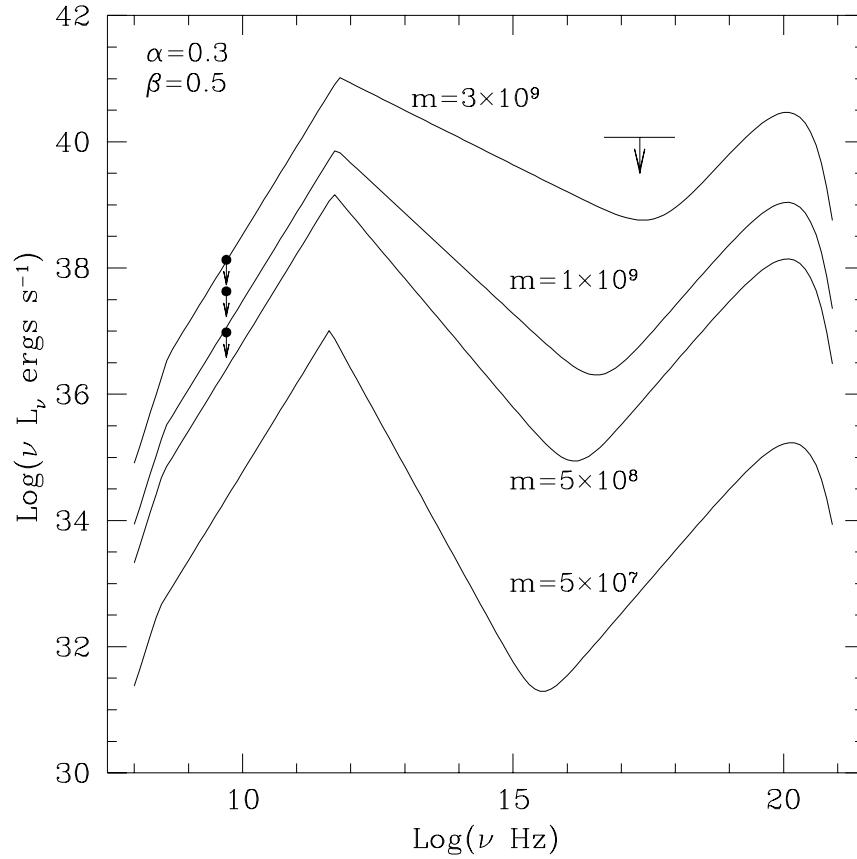


FIG. 5.—Spectra for  $m = (0.5, 5, 10, 30) \times 10^8$ , and their corresponding  $\dot{m}$  given by eq. (56). The bar and arrow represent the 0.2–4 keV upper bounds for the X-ray core emission from the bright elliptical galaxies given in Table 2. The upper bounds in the radio are the unresolved compact core fluxes (Wrobel 1991).

radius  $a_x$  and temperature  $T_7$  were also taken from Trinchieri et al. (1986). Using equation (57) and the best-fit parameters, Table 2 shows the upper limits for black hole masses using Bondi accretion. These limits are much too low to be consistent with expected masses.

### 6.3. Advection-dominated Accretion

We now show, as suggested by Fabian & Rees (1995), that advection-dominated accretion resolves this problem. Using the scaling laws derived here, we can estimate upper limits to the black hole masses. From equation (56), we find that for black hole masses of  $\sim 10^{8-10} M_\odot$ ,  $\dot{m} \sim 10^{-3}$  to  $10^{-5}$ , and we are in the regime where the total luminosity is determined by equation (49). We also expect  $\alpha_c > 1$  for these systems and therefore can set  $g(\theta_e) \sim 1$  in equation (49) (see equation [40]). Setting  $c_1 = 0.5$ ,  $c_3 = 0.3$ ,  $\beta = 0.5$ ,  $r_{\min} = 3$ , equation (49) gives

$$L_{\text{ADAF}} \simeq \eta_{\text{eff}} 0.20 \dot{M} \left( \frac{\dot{m}}{\alpha^2} \right) c^2 \text{ ergs s}^{-1}. \quad (58)$$

This is the total luminosity that is emitted over 8 orders in magnitude of frequency. Assuming that a fraction,  $\eta_x$ , of this energy is radiated into the 0.2–4.0 keV band in the X-rays (Trinchieri et al. 1986), the luminosity in this band from the advection-dominated disk is simply  $L_{b\text{ADAF}} = \eta_x L_{\text{ADAF}}$ . Multiplying equation (55) by  $0.20 \eta_x \dot{m}/\alpha^2$  gives

$$\frac{L_{b\text{ADAF}}}{L_x} = 4.3 \times 10^{-5} \eta_x \left( \frac{\alpha_b^4}{\alpha^2} \right) (M_8^3 a^3 T_7^3)^{-1} T_7^{-1/2}. \quad (59)$$

Taking  $\alpha_b = 0.5$ , as in equation (57), and  $\alpha = 0.3$ , a typical value for advection models, equation (59) becomes

$$M_8 \simeq 32.2 \eta_x^{-1/3} \left( \frac{\alpha}{0.3} \right)^{2/3} \left( \frac{L_{b\text{ADAF}}}{L_x} \right)^{1/3} a T_7^{7/6}. \quad (60)$$

The last column in Table 2 shows upper bounds for the masses of the black holes in these galaxies using  $\eta_x = 1$  (a very conservative estimate) from the advection models. The upper limits shown are much higher than those of Fabian & Canizares (1988). A maximum value of  $\eta_x$  is obtained by arbitrarily setting  $\alpha_c = 1$ . This gives a flat spectrum on a  $\nu L_\nu$  plot, and since the total emission occurs over eight orders in magnitude of frequency and the observations are made only in the 0.2–4.0 keV band,  $\sim 1$  order in magnitude,  $\eta_x \lesssim 1/8 \simeq 0.13$ . This corresponds to increasing the upper limits in Table 2 by a factor of  $\sim 2$ . Furthermore, since  $\alpha_c > 1$  in these systems,  $\eta_x$  would probably be significantly lower, and this would raise the upper limits

even more. Figure 5 shows the upper limits of the core X-ray emission, from the galaxies in Table 2, in the 0.2–4 keV band and shows the spectrum from an advection-dominated disk for  $m = (0.5, 5, 10, 30) \times 10^8$ , with the corresponding  $\dot{m}$  given by equation (56), and  $\alpha = 0.3$ ,  $\beta = 0.5$ . Clearly, the value of  $\eta_X \lesssim 0.13$ , and easily allows for black hole masses  $\lesssim 10^{10} M_\odot$  at the centers of bright ellipticals, consistent with the idea that bright elliptical galaxies do host dead quasars.

## 7. DISCUSSION AND CONCLUSION

The advection models are very robust in that they have very characteristic spectra: a  $\nu^{1/3}$  slope in the radio regime, a submillimeter-to-X-ray Compton spectrum, and a bremsstrahlung spectrum. If we assume that a system is going through advection-dominated accretion, as in the case of the elliptical galaxies above, we can make predictions of what the spectrum should look like. With  $\alpha$ ,  $\beta$  fixed, and  $\dot{m}$  given by equation (56), the only free parameter that can be varied is the mass. Once this is fixed, the entire spectrum is completely determined. The radio spectrum in these elliptical galaxies should follow a  $\sim \nu^{1/3}$  slope, which extends up to a peak frequency,  $\nu_p$ . Radio observations of these galaxies would therefore determine their core masses and would lead to testable predictions for the X-ray fluxes. Note that the inclusion of a thin disk might change the optical and ultraviolet region of the spectrum but would not affect the strong correlation between the radio and X-ray fluxes (see, e.g., Lasota et al. 1996). Observations in the radio of these elliptical galaxies have been done (Wrobel 1991). Although Wrobel (1991) observes weak jets at the cores of these elliptical galaxies, upper limits to the unresolved compact core emission have been obtained. These upper bounds are shown in Figure 5. We see that the radio bounds are quite consistent with black hole masses  $m \gtrsim 10^9$ . The masses of NGC 4636, 4649, and 4472 in this simple description are constrained to be less than  $10^9$ ,  $2 \times 10^9$ , and  $3 \times 10^9 M_\odot$ , respectively. This is a remarkable testable feature of the advection models: to explain the entire spectra of these systems using few free parameters.

Interestingly, Slee et al. (1994) have observed radio spectra in other bright elliptical galaxies and obtain an average radio spectral index of 1/3. If this is emission from a compact core, it is generally accepted to be from a nonthermal source of electrons (see, e.g., Duschl & Lesch 1994). However, if these low-luminosity systems are advection-dominated flows, then the thermal self-absorbed synchrotron radiation from these models naturally give rise to the characteristic 1/3 spectrum produced by optically thin nonthermal synchrotron emission.

Another interesting application of these models is to explain low-luminosity active galactic nuclei (AGNs; Narayan 1996). We again use the strong correlation between the radio and X-ray fluxes. The luminosity of quasars in the X-rays are  $\gtrsim 10^{44}$  ergs  $s^{-1}$ , and their accretion rates are  $> \dot{m}_{\text{crit}}$ . However, as the accreting rate decreases and falls below  $\dot{m}_{\text{crit}}$ , the accreting gas might prefer to follow an advection flow (Narayan & Yi 1995b). Since  $\dot{m}_{\text{crit}}$  is independent of  $m$ , all AGNs making this transition would have very hard X-ray spectra with spectral indices  $\sim 0.7$ , since  $\alpha_c < 1$ . Since the temperature of all systems near  $\dot{m}_{\text{crit}}$  are well determined (see Figure 2 and § 5.1.2), we can get a good estimate of  $\dot{m}$  using equation (34). This could then be combined with the X-ray luminosity to give an estimate of the mass of the central object. With the mass, accretion rate, and temperature of these systems, the advection-dominated models can be used to make predictions of the radio spectrum from these sources. Recently, Ho (1996) has obtained observations of nearby galaxies that show AGN-like spectral lines, are underluminous, and have steep X-ray spectra. Observations in the radio of these galaxies would not only serve as a test for the advection models but would also independently determine the masses of the central objects.

We have shown that the general properties of optically thin advection-dominated flows can be easily understood through simple scaling laws. The spectra that these models produce can be reproduced fairly well from a basic knowledge of the three electron cooling processes. For high  $\dot{m}$ , the Compton power is the dominant source of cooling, which gives a very hard X-ray spectrum. In the opposite limit, for low  $\dot{m}$ , synchrotron cooling dominates the cooling, and most of the energy is emitted in the radio. The bremsstrahlung power is negligible but, depending on the amount of Compton power, can dominate the X-ray emission.

These results have been applied to determine, as suggested by Fabian & Canizares (1988), and more recently by Fabian & Rees (1995), whether dead quasars are at the centers of elliptical galaxies. We have found that if these are advection-dominated systems, which is most likely due to the low accretion rates, then the upper limits are much higher,  $M \lesssim 5 \times 10^9 M_\odot$ , than those determined by Fabian & Canizares (1988),  $M \lesssim 3 \times 10^7 M_\odot$ . Therefore, we are allowed to have black hole masses of  $M \lesssim 10^{10} M_\odot$  at the centers of bright ellipticals as required by independent arguments.

The advection models are constantly tested by observations. Since there are few free parameters in the model and since the predicted spectrum ranges over all observable frequencies, failure to comply with any observation would pose serious problems. All the observations on putative 1 to  $10^9 M_\odot$  advection-dominated black hole systems have so far agreed quite well with predictions.

The author thanks Ramesh Narayan for many useful discussions and comments and the referee, A. C. Fabian, for helpful suggestions. This work was supported by NSF grant AST 9423209.

## APPENDIX A

### ANALYTIC APPROXIMATION TO $q^{\text{ie}}$

The energy transfer rate from the ions to electrons via Coulomb collisions is given by Stepney & Guilbert (1983)

$$q^{\text{ie}} = 5.61 \times 10^{-32} \frac{n_e^2(T_i - T_e)}{K_2(1/\theta_e)K_2(1/\theta_i)} \left[ \frac{2(\theta_e + \theta_i)^2 + 1}{(\theta_e + \theta_i)} K_1\left(\frac{\theta_e + \theta_i}{\theta_e \theta_i}\right) + 2K_0\left(\frac{\theta_e + \theta_i}{\theta_e \theta_i}\right) \right] \text{ ergs cm}^{-3} \text{ s}^{-1}. \quad (\text{A1})$$

The following identities hold for the temperature range of interest:

$$10^9 < T_i < 10^{12}, \quad 10^{-4} < \theta_i < 10^{-1}, \quad 10 < \theta_i^{-1} < 10^4, \quad (\text{A2})$$

and

$$10^9 < T_e < 10^{10}, \quad 0.17 < \theta_e < 1.7, \quad 0.6 < \theta_e^{-1} < 6. \quad (\text{A3})$$

The arguments of the modified Bessel functions  $K_0$  and  $K_1$  are large for these values of  $\theta_e$  and  $\theta_i$ , which enable the use of the approximation (Abramowitz & Stegun 1964, formula [9.7.2])

$$K_n(x) \simeq \sqrt{\frac{\pi}{2x}} e^{-x} \left( 1 + \frac{4n^2 - 1}{8x} + \dots \right). \quad (\text{A4})$$

Since  $\theta_i \ll 1$ , terms of order  $O(\theta_i/\theta_e)$  can be neglected. This gives

$$K_0\left(\frac{\theta_e + \theta_i}{\theta_e \theta_i}\right) \simeq \sqrt{\frac{\pi}{2}} \left(\frac{\theta_e \theta_i}{\theta_e + \theta_i}\right)^{1/2} e^{-1/\theta_i} e^{-1/\theta_e}, \quad (\text{A5})$$

$$K_1\left(\frac{\theta_e + \theta_i}{\theta_e \theta_i}\right) \simeq \sqrt{\frac{\pi}{2}} \left(\frac{\theta_e \theta_i}{\theta_e + \theta_i}\right)^{1/2} e^{-1/\theta_i} e^{-1/\theta_e}, \quad (\text{A6})$$

$$K_2\left(\frac{1}{\theta_i}\right) \simeq \sqrt{\frac{\pi}{2}} \theta_i^{1/2} e^{-1/\theta_i}. \quad (\text{A7})$$

Equation (A1) then becomes

$$q^{\text{ie}} \simeq 5.61 \times 10^{-32} \frac{n_e n_i (T_i - T_e)}{K_2(1/\theta_e)} \left(\frac{\theta_e \theta_i}{\theta_i(\theta_e + \theta_i)}\right)^{1/2} \left[ \frac{2(\theta_e + \theta_i)^2 + 1 + 2(\theta_e + \theta_i)}{(\theta_e + \theta_i)} \right] e^{-1/\theta_e} \text{ ergs cm}^{-3} \text{ s}^{-1}, \quad (\text{A8})$$

which simplifies to

$$q^{\text{ie}} \simeq 5.61 \times 10^{-32} n_e n_i (T_i - T_e) g(\theta_e) \text{ ergs cm}^{-3} \text{ s}^{-1}, \quad (\text{A9})$$

where

$$g(\theta_e) \equiv \frac{1}{K_2(1/\theta_e)} \left( 2 + 2\theta_e + \frac{1}{\theta_e} \right) e^{-1/\theta_e}. \quad (\text{A10})$$

Values of  $g(\theta_e)$  are given in Table 1.

## APPENDIX B

### DETERMINING $x_M$

From equation (20) we have

$$\exp(1.8899 x_M^{1/3}) = 2.49 \times 10^{-10} \frac{4\pi n_e R}{B} \frac{1}{\theta_e^3 K_2(1/\theta_e)} \left( \frac{1}{x_M^{7/6}} + \frac{0.40}{x_M^{17/12}} + \frac{0.5316}{x_M^{5/3}} \right). \quad (\text{B1})$$

Since most systems of interest are highly self-absorbed,  $x_M$  will be large and therefore fairly independent of  $r$ .<sup>2</sup> In this case, we can set  $r = 3$  in equation (B1) and neglect the last two terms in the parentheses (this can be checked for self-consistency). Substituting for  $n_e$ ,  $R$ , and  $B$  from equations (5) in equation (B1) and taking logarithms on both sides gives

$$y + 1.852 \ln y \simeq 10.36 + 0.26 \ln(m\dot{m}) - 0.26 \ln[\theta_e^3 K_2(1/\theta_e)] - 0.26 \ln \left[ \left( \frac{\alpha}{0.3} \right) \left( \frac{c_1}{0.5} \right) \left( \frac{c_3}{0.3} \right) \left( \frac{1 - \beta}{0.5} \right) \right], \quad (\text{B2})$$

where

$$y = x_M^{1/3}.$$

This equation can be solved numerically, and Table 1 shows the values of  $\theta_e^3 K_2(1/\theta_e)$  for the temperature range of interest.

<sup>2</sup> Numerical calculations have shown that  $x_M \sim r^{1/15}$ , for  $r \lesssim 10^3$ .



Figure 2 shows plots of  $x_M$  as a function of  $\dot{m}$  for different values of black hole mass  $m$ , where the value of  $x_M$  is determined after solving for the equilibrium temperature in the flows (see § 5.1.1). Since  $x_M$  is weakly dependent on  $m$ ,  $\alpha$ ,  $\beta$ , but depends on  $\dot{m}$ , we have a useful formula for the dependence of  $x_M$  on  $\dot{m}$ :

$$\log x_M = 3.6 + \frac{1}{4} \log \dot{m}, \quad (\text{B3})$$

which can be used for different values of  $m$ ,  $\alpha$ , and  $\beta$  to a good approximation.

## APPENDIX C

### FORMULAE FOR $\delta = 0$

In this appendix we give formulae for  $\delta = 0$ . In § 5.1.2 we obtained an equation for the temperature for  $\alpha_c > 1$  where we neglected  $Q^{\text{ic}}$  compared with  $\delta Q^+$ . If  $\delta = 0$  or  $\dot{m} \geq 10^{-4}$ , the temperature has to be determined by setting

$$\begin{aligned} Q^{\text{ic}} = Q^- &\simeq \left(0.71 + \frac{1}{\alpha_c - 1}\right) v_p L_{v_p} \\ &\simeq A_c v_p L_{v_p}, \end{aligned} \quad (\text{C1})$$

where the first term is due to synchrotron cooling and the second is due to Compton cooling. Using equation (13) and rewriting gives

$$\frac{T_e^7}{g(\theta_e)} \simeq \frac{1.2 \times 10^{74}}{A_c} x_M^{-3} \alpha^{-1/2} \beta (1 - \beta)^{-3/2} c_1^{-1/2} c_3^{-1/2} m^{1/2} \dot{m}^{1/2} r_{\min}^{3/4}. \quad (\text{C2})$$

To simplify further,  $g(\theta_e)$  can be approximated to

$$g(\theta_e) \simeq 1.91 \times 10^{11} T_e^{-1.1464}, \quad (\text{C3})$$

which is valid for  $10^9 \text{ K} \leq T_e \leq 3 \times 10^{10} \text{ K}$  and has a maximum error of 20% at  $T_e \sim 10^9$ .<sup>3</sup> Using this approximation and canonical values of the constants gives

$$T_e \simeq \frac{2.7 \times 10^9}{A_c^{3/25}} \left(\frac{x_M}{1000}\right)^{-2/5} \left(\frac{\alpha}{0.3}\right)^{-3/50} \left(\frac{\beta}{0.5}\right)^{3/25} \left(\frac{1 - \beta}{0.5}\right)^{-1/5} \left(\frac{c_1}{0.5}\right)^{-3/50} \left(\frac{c_3}{0.3}\right)^{-3/50} \left(\frac{r_{\min}}{3}\right)^{1/10} m^{3/50} \dot{m}^{3/50} \text{ K}, \quad (\text{C4})$$

where  $0.96 \leq A_c^{3/25} \leq 1.3$ , and we have approximated the exponents to the nearest fraction.

<sup>3</sup> The error made in this approximation is reduced when taking the  $\sim$  one-seventh power to determine  $T_e$ .

## REFERENCES

- Abramowicz, M., Chen, X., Kato, S., Lasota, J. P., & Regev, O. 1995, *ApJ*, 438, L37  
 Abramowicz, M., Czerny, B., Laso, J. P., & Szuszkiewicz, 1988, *ApJ*, 332, 646  
 Abramowicz, M., & Stegun, A. I. 1965, *Handbook of Mathematical Functions* (Washington: NBS)  
 Bondi, H. 1952, *MNRAS*, 112, 195  
 Canizares, C. R., Fabbiano, G., & Trinchieri, G. 1987, *ApJ*, 312, 503  
 Dermer, C. D., Liang, E. P., & Canfield, E. 1991, *ApJ*, 369, 410  
 Duschl, W., & Lesch, H. 1994, *A&A*, 286, 431  
 Esin, A. 1997, *ApJ*, submitted  
 Fabian, A. C., & Canizares, C. R. 1988, *Nature*, 333, 829  
 Fabian, A. C., & Rees, M. J. 1995, *MNRAS*, 277, L55  
 Frank, J., King, A., & Raine, D. 1992, *Accretion Power in Astrophysics* (Cambridge: Cambridge Univ. Press)  
 Haswell, A. C., Robinson, L. E., Horne, K., Stiening, F. R., & Abbott, M. C. T. 1993, *ApJ*, 411, 802  
 Ho, C. L. 1996, in *ASP Conf. Proc. 103, The Physics of LINERS in View of Recent Observations*, ed. M. Eracleous, P. A. Koratkar, C. L. Ho, & C. Leitherer, C. (San Francisco: ASP), 103  
 Lasota, J. P., Abramowicz, M. A., Chen, X., Krolik, J., & Narayan, R., & Yi, I. 1996, *ApJ*, 462, 192  
 Mahadevan, R., Narayan, R., & Yi, I. 1996, *ApJ*, 465, 327  
 Matsumoto, R., Kato, S., & Fukue, J. 1985, in *Proc. Symposium on Theoretical Aspects of Structure, Activity, and Evolution of Galaxies: III*, ed. S. Aoki, M. Iye, & Y. Yoshii (Tokyo: Tokyo Astron. Obs.), 102  
 Narayan, R. 1996, *ApJ*, 462, 136  
 Narayan, R., McClintock, J. E., & Yi, I. 1996a, *ApJ*, 457, 821  
 Narayan, R., & Yi, I. 1994, *ApJ*, 428, L13  
 ———. 1995a, *ApJ*, 444, 231  
 ———. 1995b, *ApJ*, 452, 710  
 Narayan, R., Yi, I., & Mahadevan, R. 1995, *Nature*, 374, 623  
 ———. 1996b, *A&A*, in press  
 Rees, M. J., Begelman, M. C., Blandford, R. D., & Phinney, E. S. 1982, *Nature*, 295, 17  
 Rybicki, G., & Lightman, A. 1979, *Radiative Processes in Astrophysics* (New York: John Wiley & Sons)  
 Shapiro, S. L., Lightman, A. P., & Eardley, D. M. 1976, *ApJ*, 204, 187  
 Slee, O. B., Sadler, E. M., Reynolds, J. E., & Ekers, R. D. 1994, *MNRAS*, 269, 928  
 Soltan, A. 1982, *MNRAS*, 200, 115  
 Stepney, S., & Guilbert, P. W. 1983, *MNRAS*, 204, 1269  
 Svensson, R. 1982, *ApJ*, 258, 335  
 Trinchieri, G., Fabbiano, G., & Canizares, C. R. 1986, *ApJ*, 310, 637  
 van den Bosch, F. C., & van der Marel, R. P. 1995, *MNRAS*, 274, 884  
 van der Marel, R. 1995, in *IAU Symp. 171, New Light on Galaxy Evolution*, ed. R. Bender, & R. L. Davies (Dordrecht: Kluwer), 117  
 Wandel, A., & Mushotzky, R. F. 1986, *ApJ*, 306, L61  
 Wrobel, M. J. 1991, *AJ*, 101, 127